

Electronic Density of States of Atomically Resolved Single-Walled Carbon Nanotubes: Van Hove Singularities and End States

Philip Kim, Teri W. Odom, Jin-Lin Huang, and Charles M. Lieber

Harvard University, 12 Oxford Street, Cambridge, Massachusetts 02138

(Received 24 August 1998)

The electronic densities of states of atomically resolved single-walled carbon nanotubes have been investigated using scanning tunneling microscopy. Peaks in the density of states due to the one-dimensional nanotube band structure have been characterized and compared with tight-binding calculations. In addition, tunneling spectroscopy measurements recorded along the axis of an atomically resolved nanotube were found to exhibit new, low-energy peaks in the density of states near the tube end. Calculations suggest that these features arise from the specific arrangement of carbon atoms that close the nanotube end. [S0031-9007(99)08406-9]

PACS numbers: 71.20.Tx, 61.16.Ch, 73.20.At

The electronic properties of single-walled carbon nanotubes (SWNTs) are currently the focus of considerable interest [1]. According to theory [2–4], SWNTs can exhibit either metallic or semiconducting behavior depending on diameter and chirality. Recent scanning tunneling microscopy (STM) studies of SWNTs [5,6] have confirmed this predicted behavior and have reported peaks in the density of states (DOS), Van Hove singularities (VHS), which are believed to reflect the one-dimensional (1D) band structure of the SWNTs. A detailed experimental comparison with theory has not been carried out, although such a comparison is critical for advancing our understanding of these fascinating materials. For example, chiral SWNTs have unit cells that can be significantly larger than those of achiral SWNTs of similar diameter, and thus chiral tubes may exhibit a larger number of VHS than achiral ones [7]. Recent theoretical work [8,9] suggests, however, that semiconducting (or metallic) SWNTs of similar diameters will have a similar number of VHS near the Fermi level, independent of chiral angle. In addition, the electronic properties of localized SWNT structures, including end caps, junctions, and bends [10–13], which are essential to proposed device applications, have not been characterized experimentally in atomically resolved structures.

In this Letter, we report STM investigations of the electronic structure of atomically resolved SWNTs and compare these results with tight-binding calculations. Significantly, we find that the VHS in the DOS calculated using a straightforward zone-folding approach agree with the major features observed in our experiments. We have observed new peaks in the local DOS (LDOS) at a metallic SWNT end and have compared these results to calculations. This analysis suggests that the new peaks are associated with a specific topology required to cap the SWNT. The implications of these results and important unresolved issues are discussed.

Experimental procedures are described elsewhere in detail [6,14]. In brief, SWNT samples were prepared by laser vaporization [15], purified and then deposited onto

a Au(111)/mica substrate. Immediately after deposition, the sample was loaded into a UHV STM that was stabilized at 77 K; all of the experimental data reported in this Letter were recorded at 77 K. Imaging and spectroscopy were carried out in the constant current mode using etched tungsten tips with the bias voltage (V) applied to the tip. Spectroscopy measurements were made by recording and averaging five to ten tunneling current (I) versus V (I - V) curves at specific locations on atomically resolved SWNTs. The feedback loop was open during I - V measurements with the set point the same as during imaging. The conductance dI/dV was obtained by numerical differentiation.

An atomically resolved STM image of several SWNTs is shown in Fig. 1(a). The upper isolated SWNT rests on the Au surface and is on the edge of a small rope that contains about ten nanotubes. Below we concentrate on this individual SWNT. The diameter and chiral angle measured for this tube were 1.35 ± 0.1 nm and $-20 \pm 1^\circ$, respectively. These values are consistent with (13, 7) and (14, 7) indices [6,14], where (13, 7) and (14, 7) are expected to be metallic and semiconducting, respectively. The I - V data exhibit metallic behavior with relatively sharp, steplike increases at larger $|V|$ [Fig. 1(b)]. The I - V curves have a finite slope, and thus the normalized conductance $(V/I)(dI/dV)$, which is proportional to the LDOS, has an appreciable nonzero value around $V = 0$ as expected for a metal [Fig. 1(b) inset]. This suggests that the (13, 7) indices are the best description of the tube (we address this point further below). At larger $|V|$, several sharp peaks are clearly seen in dI/dV and $(V/I)(dI/dV)$ vs V . These peaks were observed in four independent data sets recorded at different positions along this atomically resolved tube [but not on the Au(111) substrate], and thus we believe these reproducible features are intrinsic to the SWNT. We attribute these peaks to the VHS resulting from the extremal points in the 1D energy bands [16].

The availability of spectroscopic data for atomically resolved nanotubes represents a unique opportunity for comparison with theory. In this regard, we have

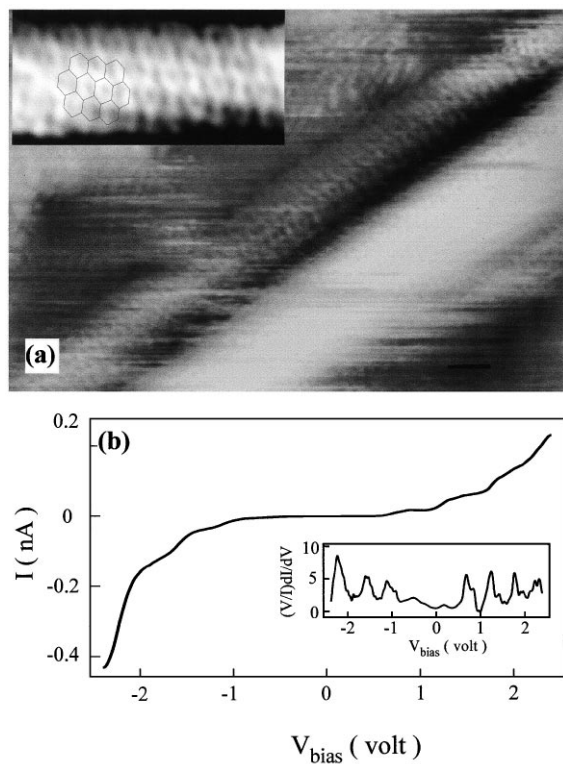


FIG. 1. (a) STM image of SWNTs recorded with $I = 0.12$ nA and $V = 550$ mV. Tunneling spectra were recorded on the isolated upper tube. The black scale bar is 1 nm. The inset shows an atomic resolution image of this tube. A portion of a hexagonal lattice is overlaid to guide the eye. (b) I - V data recorded on the SWNT in (a). The inset depicts the normalized conductance $(V/I)dI/dV$.

calculated the band structure of a (13,7) SWNT using the tight-binding method. If only π and π^* orbitals are considered, the SWNT band structure can be constructed by zone folding the 2D graphene band structure into the 1D Brillouin zone specified by the (n,m) indices [1]. Figure 2(a) shows the graphene π band structure around the corner point (\mathbf{K}) of the hexagonal Brillouin zone. For the metallic (13,7) tube, the degenerate 1D bands that cross \mathbf{K} result in a finite DOS at the Fermi level. Note that the energy dispersion is isotropic (circular contours) near \mathbf{K} and becomes anisotropic (rounded triangular contours) away from \mathbf{K} . Therefore, the first two VHS in the 1D bands closest to \mathbf{K} (depicted by \blacktriangle and \blacktriangledown) have a smaller splitting in the energy than the next two VHS (depicted by \blacksquare and \blacklozenge) due to the increasing anisotropy. If the energy dispersion were completely isotropic, both sets of peaks would be degenerate. Values for the hopping integral, $V_{pp\pi}$, reported in the literature range from about 2.4 to 2.9 eV [1,2,5,6,8,17]. We use a value of 2.5 eV determined from previous measurements of the energy gap vs diameter [6].

Our data show relatively good agreement with the DOS for a (13,7) tube calculated using the zone-folding approach [Fig. 2(b)]. The agreement between the experi-

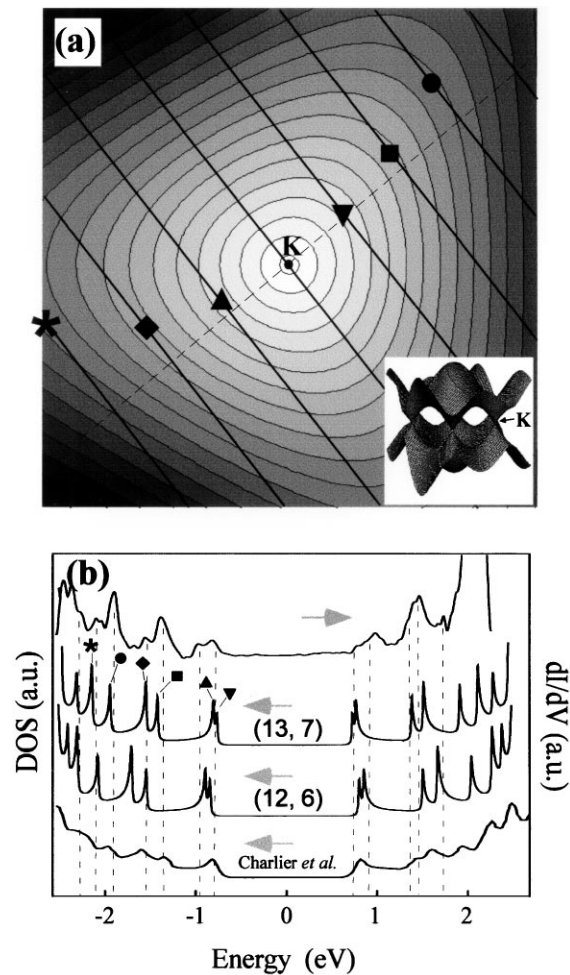


FIG. 2. (a) Energy dispersion of the π band of a graphene sheet near \mathbf{K} . The solid lines correspond to the (13,7) 1D bands obtained by zone folding. Symbols are located at the positions where VHS occur in these 1D bands. The inset depicts a three-dimensional view of the graphene π/π^* bands. (b) Comparison of the DOS obtained from experiment (upper curve) and a π -only tight-binding calculation for the (13,7) SWNT (second curve from top). The broken vertical lines indicate the positions of VHS in the tunneling spectra after consideration of thermal broadening convolution. The symbols correspond to the VHS shown in (a). The calculated DOS for a (12,6) tube and an independent calculation for a (13,7) tube [9] are included for comparison.

mental and calculated VHS is especially good below the Fermi energy (E_F) where the first seven peaks correspond well. Deviations between experimental data and calculations are larger above than below E_F . The observed differences may be due to band repulsion, which arises from curvature-induced hybridization or surface-tube interactions, which were not accounted for in our calculations. Detailed *ab initio* calculations [18] have shown that the effect of curvature-induced hybridization is much larger in π^*/σ^* than π/σ orbitals. Bands above E_F are thus more susceptible to hybridization effects, and this could explain the deviations observed for the empty states. In the future, comparison between experiment and more

detailed calculations should help to (a) resolve such subtle but important points and (b) understand how intertube and tube-substrate interactions affect SWNT band structure.

In addition, we have compared these results to a recent $\sigma + \pi$ calculation for a (13,7) SWNT [9] and a π -only calculation for a closely related set of indices. The bottom curve in Fig. 2(b) is adopted from [9] and was obtained using $2s$ and $2p$ orbitals. Although detailed comparison is difficult due to the large DOS broadening, all peaks within ± 2 eV match well with our π -only calculation. This comparison suggests that curvature-induced hybridization is only a small perturbation within the experimental energy scale ($|V| < 2$ V) for the (13,7) tube. We have also investigated the sensitivity of the DOS to (n, m) indices by calculating the DOS of the next closest metallic SWNT to our experimental diameter and angle, that is, a (12,6) tube. Significantly, the calculated VHS for this (12,6) tube deviate much more from the experimental DOS peaks than in the case of the (13,7) tube [Fig. 2(b)]. We believe that this analysis not only substantiates our assignment of the indices in Fig. 1(a) but, more importantly, demonstrates the sensitivity of the detailed DOS to subtle variations in diameter and chirality.

Finally, we have investigated the electronic structure of the ends of atomically resolved SWNTs. Analogous to the surface states in bulk crystals [19], resonant or localized states are expected at the ends of nanotubes [10]. In accordance with Euler's rule, a capped end should contain six five-membered carbon rings (pentagons). The presence of these topological defects can cause dramatic changes in the LDOS near the end of a nanotube [20]. Previous STM studies of multiwalled nanotubes [13] reported localized states at the tube ends, although the atomic structure of the tubes was not resolved. To the best of our knowledge, STM studies of the ends of SWNTs have not been reported. Figure 3(a) shows an atomically resolved image of the end of an isolated SWNT that has also been characterized spectroscopically. The rounded structure exhibited in this and bias-dependent images [e.g., Fig. 4(a) insets] suggest strongly that the end is closed, although the atomic structure cannot be obtained since the tube axis is parallel to the image plane. These images enable us to assign the nanotube (13, -2) indices [the left-handed counterpart to an (11,2) tube]. The expected metallic behavior of the (13, -2) tube was confirmed in $(V/I)dI/dV$ data recorded away from the end [\blacktriangle , Figs. 3(a) and 3(d)]. Significantly, spectroscopic data recorded at and close to the SWNT end [\bullet and \blacktriangledown , Figs. 3(a) and 3(d)] show two distinct peaks at 250 and 500 mV that decay and eventually disappear in the bulk DOS recorded far from the tube end (\blacktriangle). The peaks were observed in ten independent data sets recorded at the tube end and are very reproducible.

To investigate the origin of these new spectroscopic features, we carried out tight-binding calculations for a

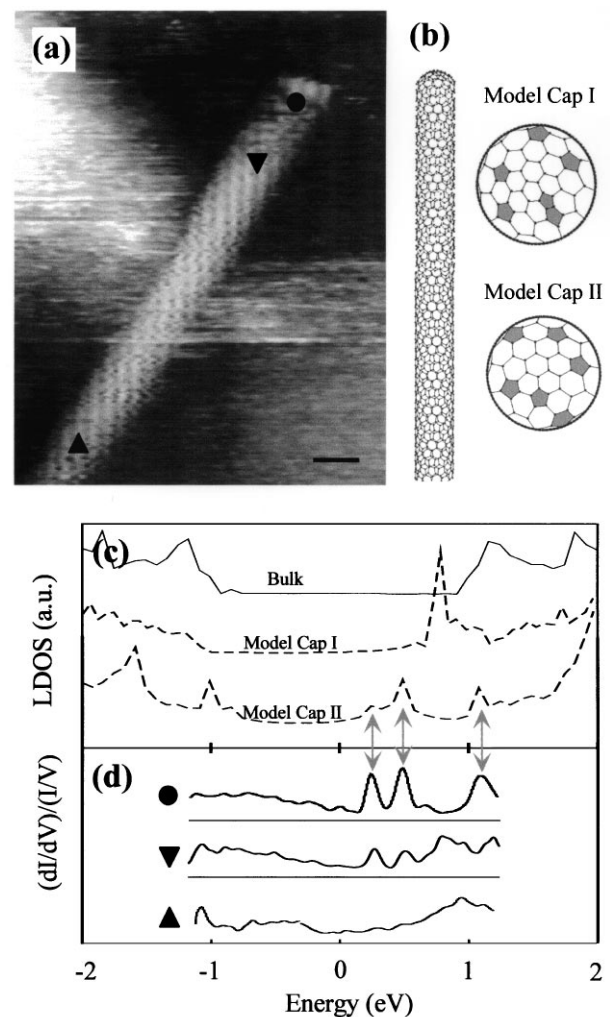


FIG. 3. (a) STM image of the end of a SWNT recorded with $I = 0.15$ nA and $V = 750$ mV. The scale bar is 1 nm, and the symbols (\bullet , \blacktriangledown , and \blacktriangle) correspond to the locations where the tunneling spectra in (d) were recorded. (b) A model (13, -2) SWNT with two different cap structures; the pentagons in the caps are shaded gray. (c) LDOS obtained from tight-binding calculations on capped (13, -2) tubes. The solid and dashed curves correspond to the calculated bulk DOS and end DOS of cap I and cap II, respectively. (d) Experimental tunneling spectra from the end (\bullet), near the end (\blacktriangledown), and far from the end (\blacktriangle). Similar features in \bullet , \blacktriangledown , and cap II are highlighted by gray arrows.

(13, -2) model tube with different end caps [Fig. 3(b)]. All of the models exhibit a bulk DOS far from the end [solid curve, Fig. 3(c)]; however, near the end, the LDOS show pronounced differences from the bulk DOS: Two or more peaks appear above E_F , and these peaks decay upon moving from the end of the bulk. Figure 3(b) shows two representative cap models. These models were chosen to illustrate the relatively large peak differences for caps closed with isolated versus adjacent pentagons. These topological configurations are not unique, although additional calculations show that other isolated (adjacent) pentagon configurations have similar LDOS. Significantly,

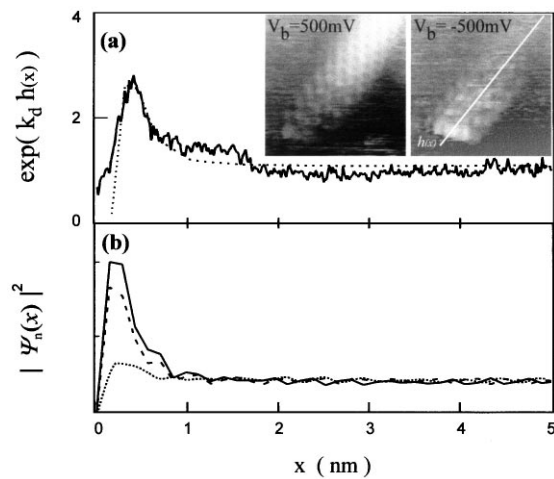


FIG. 4. (a) (insets) STM images recorded at different voltages on the SWNT end in Fig. 3. The white line indicates the $h(x)$ cross section. The solid line in (a) corresponds to $\exp[k_d h(x)]$, where $k_d = 2 \text{ \AA}^{-1}$, and the dotted line is the integrated LDOS (0–500 meV) from our calculation. (b) The solid, broken, and dotted lines depict the wave function probability (arbitrary units), $|\Psi_n(x)|^2$, of cap II as a function of position x for eigenenergies of 500, 250, and 320 meV, respectively.

the LDOS obtained from the calculation for cap II shows excellent agreement with the measured LDOS at the tube end, while cap I does not [Figs. 3(c) and 3(d)]. The positions of the two end LDOS peaks as well as the first band edge of cap II match well with those from the experimental spectra. These results suggest that the arrangement of pentagons is responsible for the observed DOS peaks at the SWNT end and are thus similar to conclusions drawn from measurements on multiwalled nanotubes that were not atomically resolved [13].

The nature of the DOS peaks at the nanotube end was further investigated using bias-dependent STM imaging. At the bias of the strong DOS peak, -500 mV , the tip-nanotube separation $h(x)$ decays with increasing x , where x is the distance from the tube end [Fig. 4(a)]. As indicated in Fig. 4(a), $\exp[k_d h(x)]$, which is proportional to the integrated LDOS [21], sharply increases around the end of the tube and then decays with a length scale of about 1.2 nm. Our tight-binding calculation suggests that this decay can be attributed to resonant end states. Wave functions whose eigenenergies correspond to the LDOS peaks (250, 500 meV) decay exponentially from the end into the bulk but retain a finite magnitude [Fig. 4(b)]; this type of decay is a signature of a resonant state [19]. Note that $h(x)$ does not decay at V far from the resonance [e.g., Fig. 3(a)], nor do wave functions with eigenenergies away from the LDOS end peaks decay with x [Fig. 4(b)]. Resonant end states in metallic tubes could serve an important function in electronic devices by improving the contact between nanotubes and electrodes.

In summary, we have characterized sharp VHS in the DOS of atomically resolved SWNTs using STM and have compared these data to tight-binding calculations for specific tube indices. A remarkably good agreement was obtained between experiment and π -only calculations, although deviations suggest that further work will be needed to understand fully the band structure of SWNTs in contact with surfaces. Pronounced peaks in the LDOS were also found at the end of an atomically resolved metallic SWNT. Comparison of these data with calculations suggests that the topological arrangement of pentagons is responsible for the localized features in the experiment. Such end states could be used to couple nanotubes effectively to electrodes in future nanotube-based devices.

We thank R.E. Smalley (Rice University) and C.-L. Cheung (Harvard University) for SWNT samples. T.W.O. acknowledges predoctoral fellowship support from the NSF, and C.M.L. acknowledges support of this work by the National Science Foundation (DMR-9306684).

- [1] M.S. Dresselhaus *et al.*, *Science of Fullerenes and Carbon Nanotubes* (Academic, San Diego, 1996).
- [2] J.W. Mintmire *et al.*, *Phys. Rev. Lett.* **68**, 631 (1992).
- [3] N. Hamada *et al.*, *Phys. Rev. Lett.* **68**, 1579 (1992).
- [4] R. Saito *et al.*, *Appl. Phys. Lett.* **60**, 2204 (1992).
- [5] J.W.G. Wildoer *et al.*, *Nature (London)* **391**, 59 (1998).
- [6] T.W. Odom *et al.*, *Nature (London)* **391**, 62 (1998).
- [7] M.S. Dresselhaus, *Nature (London)* **391**, 19 (1998).
- [8] C.T. White *et al.*, *Nature (London)* **394**, 29 (1998).
- [9] J.-C. Charlier *et al.*, *Phys. Rev. B* **57**, R15037 (1998).
- [10] P.H. Lambin *et al.*, *J. Phys. Chem. Solids* **58**, 1833 (1997).
- [11] L. Chico *et al.*, *Phys. Rev. Lett.* **76**, 971 (1996).
- [12] C.L. Kane *et al.*, *Phys. Rev. Lett.* **78**, 1932 (1997).
- [13] D.L. Carroll *et al.*, *Phys. Rev. Lett.* **78**, 2811 (1997).
- [14] T.W. Odom *et al.*, *J. Mater. Res.* **13**, 2380 (1998).
- [15] T. Guo *et al.*, *Chem. Phys. Lett.* **243**, 49 (1995).
- [16] The broad features observed in $(V/I)dI/dV$ near $V = 0$ do not correspond to significant changes in the DOS; the variation in dI/dV is small compared to that of the VHS occurring at the band edges. These small variations in the DOS may be attributed to the interaction between the tube and Au substrate or adjacent tubes.
- [17] C.T. White *et al.*, *Phys. Rev. B* **47**, 5485 (1993).
- [18] X. Blase *et al.*, *Phys. Rev. Lett.* **72**, 1878 (1994).
- [19] M. Lannoo and P. Friedel, *Atomic and Electronic Structure of Surfaces* (Springer-Verlag, Berlin, 1991).
- [20] R. Tamura *et al.*, *Phys. Rev. B* **52**, 6015 (1995).
- [21] If the wave function normal to the tube axis decays exponentially with a constant inverse decay length k_d , $\int_0^V dE \text{LDOS}(x, E) \propto \exp[k_d h(x)]$. k_d was obtained from experimental current versus distance measurements.